Structural Safety 85 (2020) 101955

Contents lists available at ScienceDirect

Structural Safety

journal homepage: www.elsevier.com/locate/strusafe

Probabilistic assessment of steel buildings installed with passive control devices under multi-hazard scenario of earthquake and wind

Tathagata Roy, Vasant Matsagar*

Multi-Hazard Protective Structures (MHPS) Laboratory, Department of Civil Engineering, Indian Institute of Technology (IIT) Delhi, Hauz Khas, New Delhi - 110 016, India

ARTICLE INFO

Keywords:
Earthquake
Fragility
Multi-hazard
Stochasticity
Wind

ABSTRACT

The multi-hazard effects on multi-story steel buildings equipped with energy dissipative passive vibration response control devices are investigated for their performance under earthquake- and wind-induced forces. The passive response control devices include steel bracings, viscous, and viscoelastic dampers. The buildings without and with the passive control devices are modeled as multi-degree of freedom (M-DOF) systems, with the seismic masses lumped at each floor level. The governing differential equations of motion for the uncontrolled and controlled buildings are solved by using Newmark's time integration approach. The dynamic response quantities are compared in terms of statistical distribution, which include the statistics of top floor acceleration, inter-storey drift, column base shear, and top floor displacement, for the uncontrolled and controlled buildings subjected to earthquake- and wind-induced forces. Conditional probabilities of failure are determined by overlapping the probability density function curves and conducting fragility analysis through cumulative distribution function curves to assess the effectiveness of the control devices against the natural hazards. It is observed that the design of the passive control devices employing additional damping may account for the performance of the structures under the multi-hazard scenario. Moreover, the variability in either of the demands affects the failure probability of the passively controlled structures extensively. Therefore, the probability of failure for a structure experiencing high-amplitude seismic hazard and a maximum wind speed within the critical frequency band during the design life varies largely for different damper schemes, which calls upon careful selection for design of a structure considering such multi-hazard scenario.

1. Introduction

Multiple natural hazards, such as, earthquakes, windstorms, tsunamis, landslides, etc. cause significant devastations, which are clearly observed from the past catastrophic events [18,26]. The destructive effects of these multi-hazard events include: fatalities, building damage, destructions to strategically important lifeline structures, critical service failures, and socio-economic losses. The associated consequences largely depend on the interaction and mutual concurrence of such hazards. The interacting effects of multiple hazards have direct impact on the performance and resiliency of modern critical structures [47]. Hence, interest towards the multi-hazard assessment of structures has emerged to mitigate the adverse consequences against multiple threats. However, because the multi-hazard and risk concept is a relatively nascent area of natural risk governance, there are only a few multi-risk models available as well as the experience of the practitioners in using such models is relatively limited [21]. Therefore, this novel approach has the potential to significantly improve the structural reliability in an effective manner, as the methodology would assist in understanding the hazard interaction and inter-relation effects, which is a challenging job and needs proper redressal.

Although earthquakes and heavy windstorms are independent in nature, the extent of devastations caused by these natural hazards has started demanding effective strategy for optimal design of structure and infrastructure systems explicitly under the multi-hazard effects. Significant researches have been contributed until the date to analyze and design the structures that exclusively considered the independency of the earthquake and wind hazards [37,44]. Multi-hazard assessment technique has essentially been explored towards early 21st century [50], thereby laying limited and specific guidelines in designing multiple hazard resistant structures. In recent period, there is a relative shift in assessment and design methodologies by addressing the hazards at

* Corresponding author. Tel.: +91 11 2659 1225/+91 11 2659 6433; fax: +91 11 2658 1117.
E-mail addresses: tathagata.roy@civil.iitd.ac.in (T. Roy), matsagar@civil.iitd.ac.in (V. Matsagar).
URL: http://web.iitd.ac.in/~matsagar (V. Matsagar).

https://doi.org/10.1016/j.strusafe.2020.101955
Received 10 July 2018; Received in revised form 23 February 2020; Accepted 27 February 2020
Available online 25 March 2020
0167-4730/

location of interest, and subsequently moving towards a more advanced holistic approach in order to guarantee acceptable performance under the considered multiple hazard scenarios [5]. Moreover, the strategies also indicated that counteracting effects of multiple hazards must be carefully dealt with to achieve efficient risk reduction and develop rational mitigation techniques. In this regard, probabilistic approaches were considered to evaluate the effects of combined loading scenarios in a structure for better understanding of the complex interaction and inter-relation effects [31]. Thereafter, probabilistic tools were used to establish frameworks for optimal decision-making and mitigating the risk of light-frame wood and high-rise commercial buildings under severe windstorms and earthquakes [10,27,2]. The methodologies proposed therein, provided effective frameworks for improving the performance and structural safety from threats imposed by the natural hazards. Further, optimization techniques were developed to modify the ASCE-7 (2005) by the American Society of Civil Engineers to investigate safety of structures under the multi-hazard scenario of strong wind and earthquake [38,8,6]. The original research was also extended to develop multi-hazard risk assessment (MHRA) framework to assess risk posed to highway bridges under combination of earthquake and hurricane loads [17]. Probabilistic frameworks were also developed to assess dynamic performance of offshore wind turbines for estimating significant losses under earthquakes and strong winds in multi-hazard prone regions such as, Gulf of Mexico and California coast [28]. Apart from safety and reliability of newly constructed structure or retrofit of existing structure, life-cycle cost (LCC) has been a benchmark variable to optimally design structures under multiple earthquake and wind loadings occurring during design life of structure [51,1]. In this regard, robust probabilistic tools were designed to estimate risk and life-cycle cost of lifeline structures exposed to multiple hazards [52]. Gehl and D'Ayala [13] assessed life-cycle cost from performance level in operation period of structure using system reliability methods. Recently, Venanzi et al. [48] investigated life-cycle cost of tall building under earthquake and wind loads. They concluded that although initial design may favor either earthquake or wind, life-cycle cost analysis should be performed, to address the effect of both the loading scenarios. More recently, Korswagen et al. [22] developed a framework to predict structural damage under a combination of multiple hazards. Damage states were proposed which could be used as performance objectives in future multi-hazard risk assessment.

The multi-hazard assessment is also gaining attention in assessment and design of structures with various passive control devices mostly to identify suitable mitigation options against the multiple hazards. Significant research has been contributed until the date for response control of structures against a particular hazard [12,44], especially using control devices such as, steel bracings, fluid viscous dampers, viscoelastic dampers, friction dampers, etc. These passive control devices have been effective in reducing the large responses of different structures under earthquake and wind loads separately [30,36,23]. The use of passive control devices is now being introduced in multi-hazard scenarios mainly to mitigate large deformations of structures while limiting the forces induced in it under multiple loading scenarios [42].

In recent contributions, investigation on the efficiency of retrofitted devices is conducted by optimizing the life-cycle cost of the structural system under the multiple loading scenarios [49]. Moreover, retrofitting strategies have also gained considerable attention to enhance performance and resiliency of lifeline structures under the multi-hazard scenarios [3,46]. However, it may be noted that a remedial and corrective measure for a particular hazard can worsen the response of the same structure when subjected to some other hazards [41,42]. Hence, ineffectiveness of the passive control devices consequently becomes an increased concern for structural safety under multi-hazard scenarios.

To address the above-mentioned research gap, which relates to the use of passive control devices for one hazard and its consequential effects on structural response under another hazard, the present study has been undertaken. Herein, a multi-hazard assessment of 20- and 25-storey steel buildings equipped with different passive control devices such as, steel bracing (SB), fluid viscous damper (FVD), and viscoelastic damper (VED) is conducted. Probabilistic analysis is carried out for the steel buildings with the passive control devices under a random set of scenario-based earthquake and wind loads. The specific objectives of the current investigation are: (i) to study the variation of response for the 20- and 25-storey moment resisting frame (MRF) steel buildings and alongside the building frames with passive control devices under a set of stochastic earthquake and wind loads; (ii) to assess increased risk for the chosen performance level in the limit states of failure for the MRF and the controlled steel buildings in terms of overlapped probability density function (PDF) curves; and (iii) to carry out fragility analyses by obtaining the conditional failure probability of the structures in terms of cumulative distribution function (CDF) under the earthquake and wind hazards.

Although, life-cycle cost assessment has been recommended by various researchers for optimal design of structures, this is not considered in the current scope of study. To investigate life-cycle cost of structure for optimal assessment and design, uncertainties in resistance of structure and loading scenarios are key parameters, as the required cost function includes factors relating to construction, maintenance and operation, repair of damage, etc. The current objectives explicitly deal in developing a probabilistic framework for assessing the steel buildings using different passive control devices based on the reliability study alone considering uncertainties in the loading parameters. In this regard, the latter is considered through the developed probabilistic framework to propose suitable passive control strategy for the considered steel buildings under the multi-hazard scenario of earthquake and wind.

2. Probabilistic theory and multi-hazard assessment

The combination of hazards and vulnerabilities results in determination of structural safety on probabilistic scale. Extensive research has already been conducted to define and calculate limit states of failure of structures to estimate vulnerability under a particular hazard as mentioned earlier. However, in case of the structures exposed to multi-hazard scenarios, proper guidelines are inexistent to assess the structural performance. Hence, in such multi-hazard scenarios, probability-based approach is applied, which uses the advantage of uncertainty in the system to assess the multi-hazard situation in structures.

Fig. 1 shows normalized fast Fourier transform (FFT) spectra for the considered earthquake and wind excitations. The FFT spectra are normalized with respect to their intensity measures (IMs), peak ground acceleration (PGA) and wind gust speed, in order to have a clear vision of the multi-hazard assessment concept. Scenarios pertaining to the

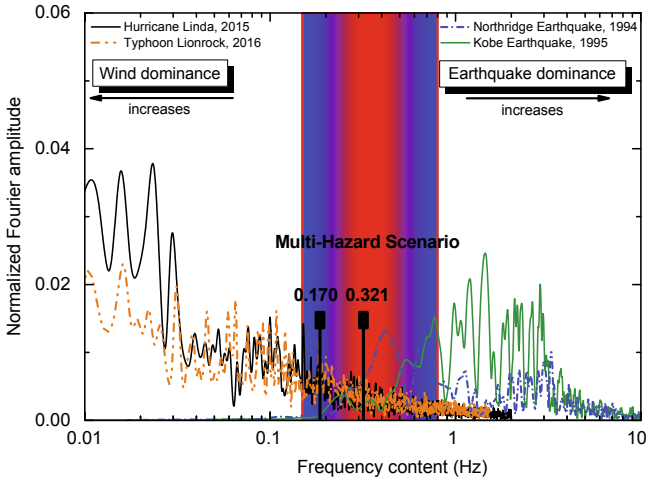

Fig. 1. Comparison of FFT amplitude spectra for considered earthquake and wind excitations.

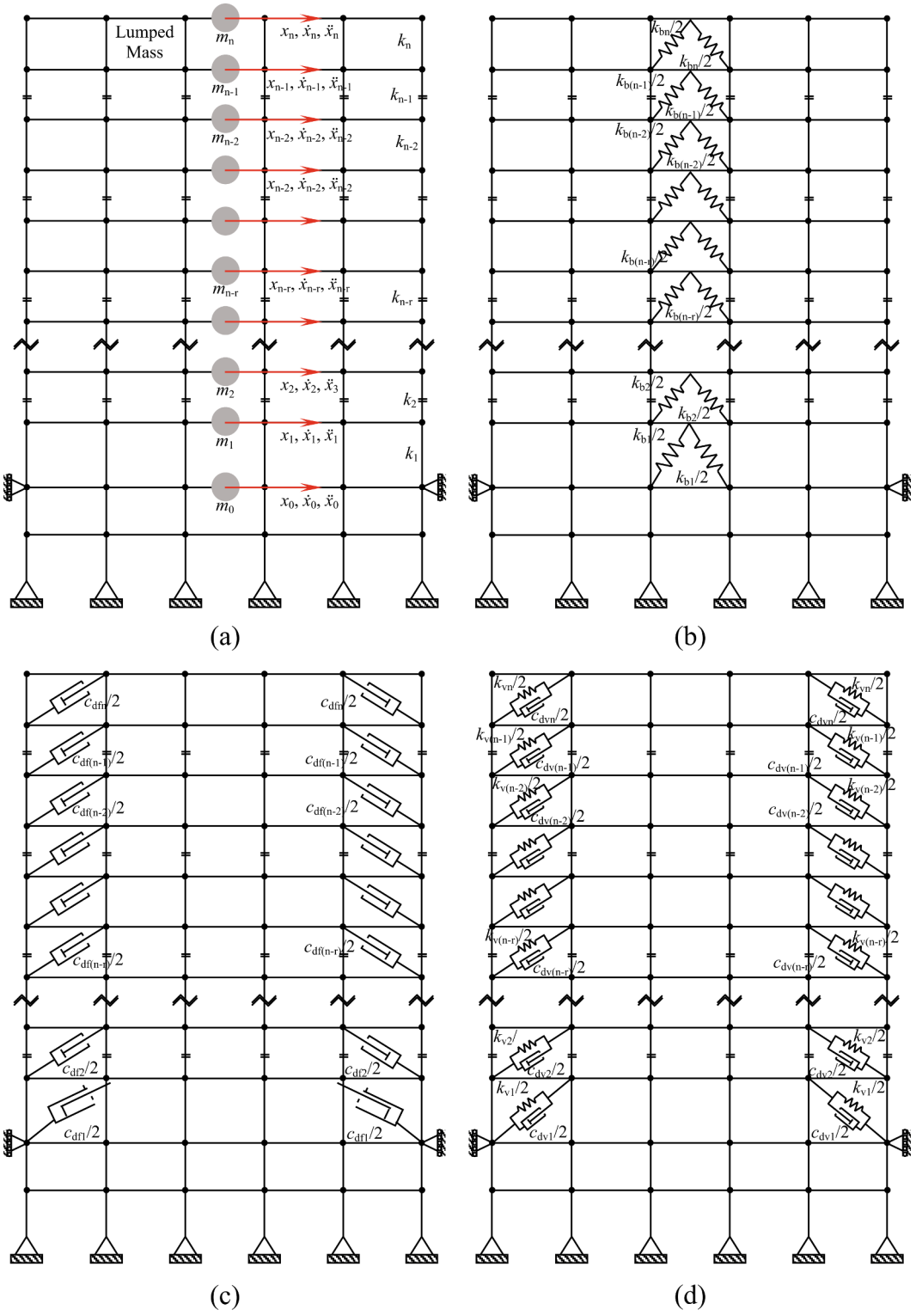

Fig. 2. Mathematical model of *n*-storey steel moment resisting frame (MRF), (b) steel braced frame (SBF), (c) fluid viscous-damped frame (FVDF), and viscoelastic-damped frame (VEDF).

occurrence of earthquake and wind hazards in design life of a structure are considered. Two natural hazards, earthquake and wind at two geographical locations are analyzed in terms of the FFT spectra of the respective time-history loadings for the multi-hazard assessment:

(a) NS component of the Northridge earthquake, 1994 recorded at the Sylmar station with peak ground acceleration (PGA) of 7.043 m/s^2, and (b) Hurricane Linda, 2015 with peak gust speed of 205 km/h occurring at the west coast of the United States of America (USA).

(a) NS component of the Kobe earthquake, 1995 recorded at the Japan Meteorological Agency (JMA) with PGA of 8.054 m/s^2, and (b) Typhoon Lionrock, 2016 with peak gust speed of 198 km/h occurring at the east coast of Japan.

The importance of this figure is significant in practical applications, especially for the practicing engineers and designers, where the effects of multiple hazards are critical in determining design loads for structures. It is well understood that seismic loads control design of new buildings with shorter periods (~0.3 – 0.9 s depending on structural configurations) rather than gusty wind loads, and vice versa. However, structural frequencies lying in the overlapped bandwidth as shown in Fig. 1 have chances to be dominated under the multiple hazards. The multi-hazard scenario for structural assessment arises when modal frequencies of structures are contained within the overlapped frequency bandwidth of the FFT spectra (Fig. 1). The sole objective of Fig. 1 is to demonstrate requirement of establishing an assessment technique for structures with a specific range of fundamental frequency which might be dominated by multiple hazards during the design life of the structures. Thus, for such structures, assessment of dynamic behavior is important for further comparison of vulnerability under the multi-hazard scenario of earthquake and wind hazards.

Let E and W be the random variables associated respectively with the occurrence of the earthquake and wind events. During these unrelated events, if the capacity C of structural members is less than the demand D posed due to individual earthquake and wind loads, then the failure probability can be expressed as,

$$p_f = \sum_{e=0}^{\infty} \sum_{w=0}^{\infty} p(C < D|E, W) p_E(E = e_L) p_W(W = w_L) \tag{1}$$

where $p_E(E = e_L)$ and $p_W(W = w_L)$ are probability mass functions of the events, E and W, respectively. Eq. (1) can be expressed in terms of total probability as,

$$p_f = \int_{e=0}^{\infty} \int_{w=0}^{\infty} F_r(e, w) g(e, w) dw de \tag{2}$$

where $F_r = \Phi[(1/\beta)\log(x/\bar{x})]$ is the conditional probability or fragility expressed as cumulative distribution function (CDF) in terms of multi-hazard demands in E and W. Here, Φ is the normal cumulative distribution function; β is the variability associated with the demands; and $\bar{x}$ is the median value of the demand, x. The joint probability function (PDF) is represented by $g(e, w)$ for the multi-hazard events, E and W. As the occurrence of earthquake does not explicitly affect the probability of occurrence of any gusty wind event, and vice versa, e and w are statistically independent. Hence, Eq. (2) can be written as,

$$p_f = \int_{e=0}^{\infty} \int_{w=0}^{\infty} F_r(e, w) g_E(e) g_W(w) dw de \tag{3}$$

where $g_E(e)$ and $g_W(w)$ are marginal PDFs.

Although, majority of the past researches have been carried out assuming mutual exclusivity of the two hazards [8], studies based on mutual occurrence of these dynamic loadings are also available. For example, recent research work carried out by Parsons et al. [35] shows that there is high probability of occurrence of earthquake of magnitude 7.1 – 7.7 in California region. Moreover, in this region a total of 2056 wind events were recorded for the last 65 years, yielding an average of 32 occurrences per year [14]. It was also observed that the average speed at Owens Valley stations in California during extreme high wind events have exceeded 40 m/s with wind gusts in excess of 50 m/s. Furthermore, data provided by National Renewable Energy Laboratory (NREL), USA, shows that California being an active seismic region, also produces the third largest wind power in the USA [28]. In another latest study, Nikellis et al. [32] have reported that the probabilities of collapse of 30 story flexible building located in Charleston, USA in a period of 50 years due to wind, earthquake, and the combined effect of wind and earthquake are respectively 0.0012, 0.0081, and 0.0094. Therefore, based on such evidences, mutual occurrence of such multiple hazards cannot be ruled out, although the hazards are independent in nature [11].

3. Mathematical modeling of the buildings with passive control devices

Mathematical models for the 20- and 25-storey steel buildings equipped without and with the passive control devices, such as, steel bracings (SB), fluid viscous dampers (FVD), and viscoelastic dampers (VED) are developed, as shown in Fig. 2, under the earthquake and wind excitations. The buildings are chosen such that the fundamental frequencies lie on the overlapped bandwidth, as shown in Fig. 1. This helps in verifying that there exists a particular band of frequencies for which the design of structures may be governed by both the earthquake and wind loads, where their robustness would be interesting to study. In this context, the variations in heights of the steel buildings are considered to study the dominance under the multi-hazard scenario. The passive control devices are chosen such that the effect of pure stiffness and/ or damping is observed under the multi-hazard scenarios of earthquake and wind. The general assumptions in modeling the buildings with the passive control devices are as follows.

(i) The steel buildings without and with the passive control devices are modeled as multi-degree of freedom (M − DOF) systems.
(ii) Seismic masses, comprised of structural and non-structural components, are lumped at respective nodes.
(iii) The floor with beam-slab interaction is modeled as rigid diaphragm in the horizontal direction.
(iv) The building is modeled with two basement floors, and the horizontal displacement of the first floor is restrained by surrounding soil and rigid concrete foundation.
(v) One degree of freedom (DOF) is considered at each floor level in the direction of earthquake and wind loads.
(vi) The steel buildings with the dampers are treated as dual systems with the moment resisting frames (MRF) as primary systems, exhibiting linear behavior and the nonlinear energy dissipating devices exhibiting elasto-plastic behavior.

The governing differential equations of motion for the uncontrolled and controlled buildings are derived hereunder and free vibration analysis is conducted to determine the modal periods. Further, the equations are solved using Newmark's time integration approach, with linear acceleration, to obtain the response history for the uncontrolled and controlled buildings.

3.1. Modeling of moment resisting frame (MRF)

The governing differential equation of motion for the steel moment resisting frame (MRF) buildings is given by,

$$[m]\{\ddot{x}(t)\} + [c]\{\dot{x}(t)\} + [k]\{x(t)\} = p(t) \tag{4}$$

where $[m]$, $[c]$, and $[k]$ are mass, damping, and stiffness matrices of the building; $\ddot{x}(t)$, $\dot{x}(t)$, and $x(t)$ are the acceleration, velocity, and displacement response of the steel MRF building obtained at each node, $\{x\} = \{x_1, x_2, x_3, ...x_{n-r}, ...x_{n-1}, x_n\}^T$, respectively; and $p(t)$ is the external force exerted on the building, either during the earthquake or wind events. On similar lines to Kaur et al. [19], when the earthquake ground-motion is applied at the base of the building, Eq. (3) for base-excited system is correspondingly modified as,

$$[m]\{\ddot{x}(t)\} + [c]\{\dot{x}(t)\} + [k]\{x(t)\} = -[m]\{r\}\ddot{u}_g \tag{5}$$

where $\{r\}$ is the influence coefficient vector; and $\ddot{u}_g$ is the applied earthquake ground-motion acceleration. Similarly, when the building is subjected to the along-wind load, Eq. (3), for mass-excited system, is correspondingly modified as,

$$[m]\{\ddot{x}(t)\} + [c]\{\dot{x}(t)\} + [k]\{x(t)\} = f(t) \tag{6}$$

where $f(t)$ is the applied force vector at the floor mass on each storey, $\{f\} = \{f_1, f_2, f_3, ...f_{n-r}, ...f_{n-1}, f_n\}^T$.

Condensing out all secondary DOFs, such as, vertical DOFs, the DOFs at spliced locations, and rotational DOFs, the mass and stiffness matrices are obtained [45,34]. Therefore, the reduced damped equation of motion becomes,

$$[\tilde{m}]\{\ddot{\tilde{x}}\} + [\tilde{c}]\{\dot{\tilde{x}}\} + [\tilde{k}]\{\tilde{x}\} = \tilde{p}(t) \tag{7}$$

where $[\tilde{m}] = \{\varphi\}^{\mathrm{T}}[\hat{m}]\{\varphi\}$ is the generalized mass matrix; $[\tilde{c}] = \{\varphi\}^{\mathrm{T}}[\hat{c}]\{\varphi\}$ is the generalized damping matrix; $[\tilde{k}] = \{\varphi\}^{\mathrm{T}}[\hat{k}]\{\varphi\}$ is the generalized stiffness matrix; $\tilde{p}(t) = \{\varphi\}^{\mathrm{T}}\{\hat{p}\}$ is the generalized force vector; $\tilde{x} = \{\varphi\}^{\mathrm{T}}\{x\}$ is the generalized displacement coordinates; and $\{\varphi\} = [\tilde{m}]^{-1}[\tilde{k}]$ is the modal matrix. The damping matrix, $[\tilde{c}]$ is obtained based on modal damping. The modal damping in each mode is proportionate to the associated frequency. The damping, ζ_{i} in the ith mode is given by,

$$\zeta_{\mathrm{i}} = \min\left\{\frac{\omega_{\mathrm{i}}}{50\omega_1}, 0.1\right\} \tag{8}$$

where ω_{i} is the natural frequency at the i^{th} mode.

3.2. Modeling of steel braced frame (SBF)

Concentric-braces (CBs) provide an effective approach to achieve relatively higher lateral stiffness in a vibrating system as well as absorb large energy through hysteretic cycles. Moreover, the CBs also provide strength in lateral direction required for seismic design of structure ([4]). Considering all the design parameters, the steel bracings are modeled using the following assumptions: (i) the steel bracings are prevented from yielding in tension, however may buckle in compression, and (ii) in-plane stiffness of the metallic braces is considered whereas out-of-plane stiffness is neglected. The horizontal braces are modeled as truss elements to transfer the lateral seismic or wind loads in compression or tension. Hence, the governing differential equation of motion for the steel braced frame (SBF) is modified with the change in lateral stiffness, $[\tilde{k}']$, where, $[\tilde{k}'] = [\hat{k}'] + [k_{\mathrm{b}}\cos^2\theta]$ is the stiffness imparted by the columns and the steel braces of the buildings (k_{b}); and, θ is the horizontal angle subtended between the steel brace and beam. On similar lines to Kaur et al. [19], for the considered configuration of the steel braces in the MRF, the axial stiffness k_{b} is represented in terms of material and geometric properties as,

$$k_{\mathrm{b}} = \frac{EA}{L} \tag{9}$$

where E is the modulus of elasticity for the steel; A is the cross-section area of the brace; and L is the effective length of the brace.

3.3. Modeling of fluid viscous-damped frame (FVDF)

In nonlinear fluid viscous damper (FVD), the output force is proportional to integer/fractional power law of velocity, which strictly corresponds to Newtonian model [15]. The range of nonlinearity affects force–deformation loop of the FVD as described by different researchers, namely, Lee and Taylor [24] and Martinez-Rodrigo and Romero [29]. The nonlinear force–velocity behavior of the FVD is given by,

$$f_{\mathrm{df}} = [c_{\mathrm{df}}]|\dot{x}|^{\alpha}\mathrm{sgn}|\dot{x}| \tag{10}$$

where f_{df} is output viscous damping force; c_{df} is damping obtained from the nonlinear viscous damper; α is constant exponent which depends on viscosity of the fluid, typically ranging from 0.2 to 1; $\dot{x}$ is relative velocity between two ends of the damper; and, sgn represents the symbolic function. Hence, the governing differential equation of motion for the fluid viscous-damped frame (FVDF), which utilizes the nonlinear force-velocity behavior under the dynamic earthquake and wind loads, is expressed as,

$$[\tilde{m}]\{\ddot{\tilde{x}}\} + [\tilde{c}]\{\dot{\tilde{x}}\} + [\tilde{k}]\{\tilde{x}\} + f_{\mathrm{df}} = \tilde{p}(t) \tag{11}$$

where $[\tilde{c}'] = [\tilde{c}] + [c_{\mathrm{df}}\cos^2\theta]$ is equivalent structural damping obtained from viscous damping of the nonlinear FVD; and $[c_{\mathrm{df}}] = 2\zeta_{\mathrm{df}}[\tilde{m}]\{\omega_{\mathrm{n}}\}$ is the damping matrix obtained from the supplemental damping where, ζ_{df} is generally taken as 5%–30% of the critical damping.

3.4. Modeling of viscoelastic-damped frame (VEDF)

Viscoelastic damper (VED) utilizes advantage of both stiffness and damping to reduce excessive vibrations caused by the earthquakes and winds. Mechanical models comprising of spring and dashpot in series or parallel are used to describe rheological properties of the VED [25]. In this study, Kelvin-Voigt model, i.e., spring-dashpot in parallel combination, is used to describe dynamic behavior of the VED. In this case, nonlinear force–deformation behavior of the VED is given by,

$$f_{\mathrm{dv}} = k_{\mathrm{v}}x^{\beta} + c_{\mathrm{dv}}\dot{x}^{\alpha} \tag{12}$$

where f_{dv} is the output viscoelastic damping force; k_{v} is the axial stiffness of the VED; c_{dv} is the damping obtained from the VED; α and β are nonlinear exponents of the damping and stiffness, respectively. Hence, the governing differential equation of motion for the viscoelastic-damped frame (VEDF), which utilizes the nonlinear force–deformation behavior of the damper under the earthquake and wind imparted loads, is given as,

$$[\tilde{m}]\{\ddot{\tilde{x}}\} + [\tilde{c}]\{\dot{\tilde{x}}\} + [\tilde{k}]\{\tilde{x}\} + f_{\mathrm{dv}} = \tilde{p}(t) \tag{13}$$

where $[\tilde{k}'] = [\hat{k}'] + [k_{\mathrm{b}}\cos^2\theta]$ is the lateral stiffness imparted by the columns of the building and the VED; $[\tilde{c}'] = [\tilde{c}] + [c_{\mathrm{df}}\cos^2\theta]$ is the equivalent structural damping obtained from the viscoelastic damping; and, $[c_{\mathrm{dv}}] = 2\zeta_{\mathrm{dv}}[\tilde{m}]\{\omega_{\mathrm{n}}\}$ is the damping matrix obtained from supplemental damping.

4. Stochasticity of the hazards

4.1. Seismic hazard

Early research used stochastic models to generate earthquake loads using empirical or physical models [33]). Seismic hazard follows stochastic models, which are functions of parameters such as, spectral acceleration of the stochastic ground-motions, duration of excitation, frequency content, epicenter distance [40]. Ground-motions play an important role in assessing the dynamic response of the structures [39]; hence, a large number of ground-motions are considered for this simulation. The ground-motions are represented by the stochastic parameters in terms of mean (μ_{e}) and standard deviation (σ_{e}), which are subsequently used in simulating the seismic response of the steel buildings. In the present study, the ground-motions are selected such that influence of non-stationary content of the ground-motions is considered to predict the realistic nature of the responses. Lognormal distribution type is assumed to study the stochasticity of the set of ground-motions, as lognormal distribution closely resembles the variation in dataset, as stated by Saha et al. [43]. For realistic results in this analysis, the ground-motions are scaled with respect to the peak ground acceleration (PGA), which is considered the earthquake hazard parameter here.

4.2. Wind hazard

The stochastic wind hazard at a location is expressed as a PDF of maximum wind speed for the site. The distribution function follows generalized extreme value (GEV) to predict the design wind speed (Gumbel-type distribution). The uncertainties in wind profile are typically observed in wind exposure factor, external and internal pressure coefficients, wind speed and wind directionality as per Ellingwood and Tekie [9]. The design wind load, therefore, is obtained from power spectral density matrix of the wind speed fluctuation [16]. The wind

speeds are represented by the stochastic parameters, in terms of mean, μ_w and standard deviation, σ_w. The time histories of the wind speeds are obtained thence by summing the static and fluctuating components obtained from the simulation based on Bernoulli's theorem, which is given by,

$$\bar{U}(t) = 0.5\rho C_d A[U(t) + u(t)]^2 \quad (14)$$

where ρ is air density; C_d is drag coefficient depending on shape of the object and nature of surface of contact; A is exposed area; $U(t)$ is mean speed component; and $u(t)$ is fluctuating speed component of the wind time history.

5. Numerical study

5.1. Case study of 20-storey benchmark steel building

In this study, effectiveness of the passive control devices installed in 20- and 25-storey steel buildings is investigated under the multi-hazard scenario of earthquake and wind loads. The 20-storey benchmark steel building for the SAC Phase II Steel Project was designed with the then seismic code at California region [45,34]. The present study is conducted on this theoretical 20-storey benchmark steel building with actual dimensions, and further, the benchmark building is assessed with the passive control devices to investigate their effectiveness under the multi-hazard scenario of earthquake and wind. In addition to the 20-storey benchmark steel building, a 25-storey steel building is hypothetically modeled by extending the stories of the 20-storey benchmark steel building. The 25-storey steel building is subsequently checked against the limit states of collapse and serviceability for gravity and earthquake loads as prescribed by the ASCE 7-05. The steel buildings that are equipped with either stiffness- and/or damping-based passive devices to serve as example theoretical buildings that are governed by multiple hazard scenarios. Proportional stiffness for the passive control devices assumed is 60% of the storey stiffness, and proportional damping assumed is ζ = 15% of the critical damping. Nonlinear exponent α for the FVD as well as the VED is assumed as 0.3. The nonlinear exponent of the stiffness (β) is assumed as 2 to simulate the classical Kelvin-Voigt model for the nonlinear VED. The general properties of the buildings assumed for this study are given in Table 1.

Free vibration analysis is performed for the uncontrolled and controlled steel buildings and the results are obtained in terms of the first five natural periods, which are given in Table 2. The additional stiffness provided by the SB and VED are the same as reflected in the modal periods in Table 2, as well as the additional damping provided by the FVD and VED. The 20-storey benchmark steel building with added stiffness has the lowest fundamental period; whereas, the 25-storey moment resisting frame (MRF) building frame has the highest fundamental period. The highest and the lowest fundamental frequencies of the steel buildings are shown in Fig. 1 to obtain a clear idea about the range of frequencies for the structures that are highly vulnerable under the multi-hazard scenario. It is significantly important to study the effects of modal properties of the buildings equipped with the passive control devices under the two different types of dynamic excitation, earthquake and wind. Bearing in mind that, the effect of number and placement of the passive control devices in multi-hazard scenario is not an objective of the current study, numerical investigation is conducted on the dynamic response of the steel buildings to observe the effects of earthquake and wind loads.

Table 2
Modal periods for the n-DOF system (in s).

	Mode No.	MRF	SBF	FVDF	VEDF
20-storey	1	3.86	3.11	3.86	3.11
	2	1.33	0.98	1.33	0.94
	3	0.78	0.53	0.78	0.49
	4	0.55	0.35	0.55	0.33
	5	0.42	0.26	0.42	0.25
25-storey	1	5.88	4.86	5.88	4.86
	2	2.15	1.48	2.15	1.49
	3	1.25	0.74	1.25	0.76
	4	0.89	0.46	0.89	0.50
	5	0.68	0.32	0.68	0.37

5.2. Probabilistic analysis of steel buildings

Probabilistic analysis is conducted for the 20- and 25-storey steel MRF buildings installed with the passive response control devices under a set of considered earthquake and wind loads. Here, the uncertainty only in the loading parameters is taken into consideration as it affects the design significantly. Uncertainties in resistance of the structure, i.e.,

Table 1
General properties for the n-degree of freedom (n-DOF) system of the steel moment resisting frame (MRF) building.

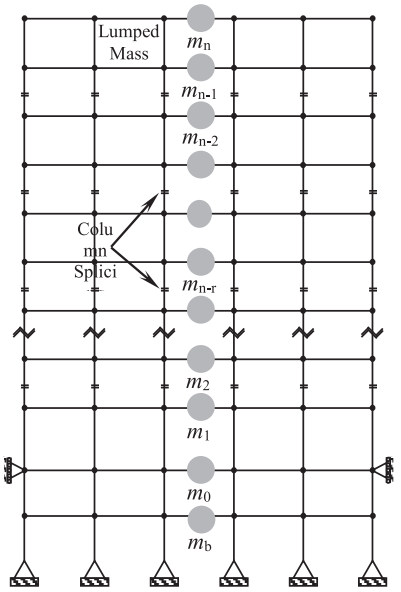

No. of Storeys	Storey Levels	Seismic Mass, m_n (kg)	Vertical/Horizontal Dimension (m)
20-storey	Basement level (n_b)	–	3.65
	Ground level (n_0)	2.66×10^5	5.49
	1st level (n_1)	2.83×10^5	3.96
	2nd (n_2) – 19th (n_{19})	2.76×10^5	3.96
	20th level (n_{20})	2.92×10^5	–
	Bay widths		6.10
25-storey	Basement level (n_b)	–	3.65
	Ground level (n_0)	2.66×10^5	5.49
	1st level (n_1)	2.83×10^5	3.96
	2nd (n_2) – 24th (n_{24})	2.76×10^5	3.96
	25th level (n_{25})	2.92×10^5	–
	Bay widths		6.10

Table 3
Statistics of the stochastically generated parameters for the earthquake and wind excitations.

Case	Distribution	Statistical Mean	Standard Deviation	Median	Skewness	Kurtosis
Earthquake	Lognormal	$\mu_e = -1.12\ g$	$\sigma_e = 0.62\ g$	0.32 g	1.77	3.87
Wind	Extreme Value	$\mu_w = 47$ m/s	$\sigma_w = 5.6$ m/s	43.33 m/s	−0.43	−0.24

geometrical details and member strengths, are ignored as the variability is relatively lower in comparison to the loading. Such importance of accounting uncertainty in the excitation parameters over the structural properties based on sensitivity analysis of the building mounted on base isolation system has been established [20]. Table 3 presents the stochastic parameters of 50 real-time earthquakes and 200 simulated wind data used to analyze the steel buildings. Negative value of the statistical mean indicates treatment of the PGA values in logarithmic domain. Although return periods of the earthquake ground-motions have significant role to play in determining the performance of a structure, the current approach does not utilize the return period by using any specific target design spectra. There is significant difficulty and challenge involved to incorporate multiple design spectra to assess the comparative performance of the steel buildings. Furthermore, the present novel probabilistic framework is more generic, which utilizes the uncertainty in the loading parameter by considering a wide range of amplitudes and non-stationary content in the earthquake data for different regions in the world. The PGA of earthquake ground-motions follows lognormal distribution; whereas, extreme value distribution is assumed to generate random variables for the wind excitations. Moreover, statistical parameters are tabulated in order to have in-depth information of the distribution of the dataset. The statistical details of the ground-motion records and wind excitations are given in Table 4. The ground-motions are scaled up to 1 g with respect to the PGA (g denotes acceleration due to gravity) for conducting the probabilistic analyses of the example steel buildings here. The acceleration and displacement response spectra of the ground-motions are plotted in Fig. 3 to compare the nature and range of the responses with the obtained fundamental periods of the steel multi-storied steel buildings.

The wind hazards are simulated using the extreme value distribution for mean speed of 47 m/s and standard deviation of 5.6 m/s to represent the scenario-based wind at California region. As California region is vastly exposed to high consequence low probability earthquake and gusty winds, majority of the historical earthquake data and the site-specific gusty speed distribution are taken from the California region, which forms a vital scenario for the multi-hazard assessment of the steel buildings under these loadings. Limit states, such as, top floor acceleration ($\ddot{x}_n$, $n = 20$ or 25), inter-storey drift (δ), base shear (V_b), and top floor displacement (x_n, $n = 20$ or 25) are chosen to quantify the probability of failure for the steel buildings. A performance level of 'moderate damage' is assumed for the limit states, with the respective limits of 2 m/s^2, 1%, 0.1 W, and 1%; where, W is total weight of the building as prescribed by Dogruel and Dargush [7]. Here, the top floor displacement is limited to 1% of the total height of the structure, which is calculated from the level of the second basement (m_0).

The above-mentioned parameters are carefully chosen as these quantities represent the limit states of collapse and serviceability of the structures. The floor accelerations developed in the superstructure are proportional to the force exerted by the structures under the dynamic earthquake and wind excitations. The serviceability criteria in terms of comfort level of the occupants of the structures is also determined from the dynamic response. The displacement as well as the inter-storey drift ratio are influential in determining the design of the lateral load carrying components of the structural systems. The performance criteria are considered deterministic to obtain the response quantities reaching or exceeding the prescribed performance levels. The peak response quantities follow lognormal distribution and further, Monte Carlo simulation is used to generate 1000 random samples based on the mean and standard deviation of the peak response reaching or exceeding the chosen limit states. The effectiveness of the control strategies for the steel buildings under the multi-hazard scenario is obtained from the overlapped area of the failure probability density functions (PDFs), $f(\cdot)$. Fragility curves, in terms of cumulative distribution functions (CDFs), are obtained to determine the probability of failure (p_f) for the steel buildings equipped with the passive control devices under the multi-hazard scenario. Fig. 4 is presented to show a detailed flowchart of the analysis steps followed to quantify the failure probability under the multi-hazard scenario of earthquake and wind. This illustration enables us to assess the effectiveness of the passive control devices for the multi-hazard scenario.

6. Discussion

6.1. Distribution of peak response data for steel buildings

Effectiveness of the control devices installed in the steel buildings is investigated from the distribution of the peak response data for the chosen performance limits under the multi-hazard scenario. The datasets are analyzed using box plots to investigate the variation in the peak responses for the uncontrolled and controlled steel buildings under the multiple dynamic loads. Moreover, the box plots also indicate sensitivity of the responses obtained for the steel buildings. It may be noted that though sensitivity analysis is not performed like Kodakkal et al. [20], the indicative sensitivity is judged from the distribution of the obtained peak responses. Figs. 5 and 6 show the box plots of the peak responses obtained for the steel buildings analyzed without and with the passive control devices under the multiple hazards. The box plots bound from 5% to 95% of the dataset to incorporate maximum skewness. The skewness of dataset is also assessed from the percentage difference in mean and median for the respective plots.

Table 4
Statistics of the 50 earthquake ground motion records and 200 simulated wind excitations.

Excitations	Parameters	Maximum	Minimum	Arithmetic Mean	Standard Deviation
Earthquake	PGA (g)	1.496	0.115	0.398	0.277
	Duration (s)	180	9.98	47.10	30.39
	Frequency [a] (Hz)	110.35	0.01	64.10	31.09
Wind	Gust Speed, U (m/s)	56.52	23.11	47	5.6
	Duration (s)	3,000			
	Cut-off Frequency (Hz)	0.5			
	Exposure Category	Urban and sub-urban area (Category-B)			

[a] Frequency content corresponding to peak FFT amplitude of the acceleration.

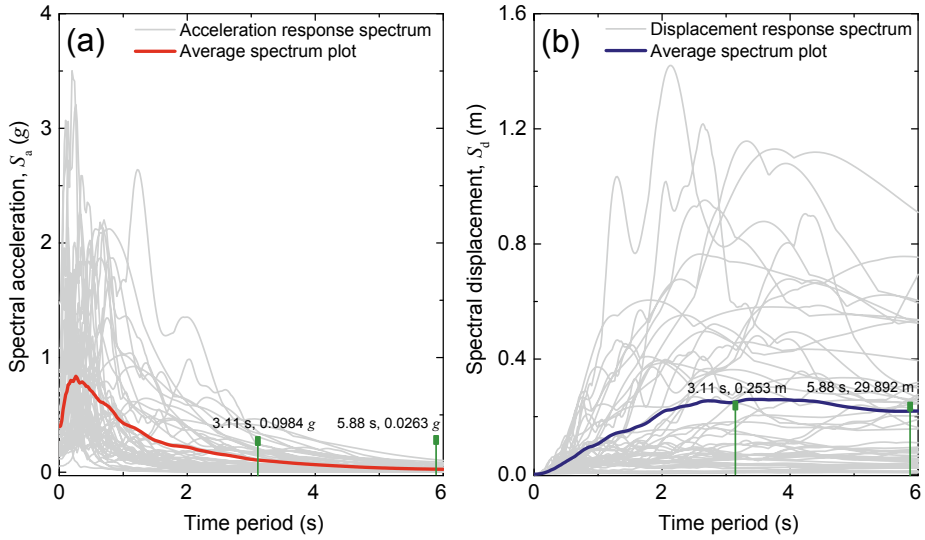

Fig. 3. (a) Acceleration and (b) displacement response spectrum plots for the 50 real time earthquake ground motions.

Fig. 5 shows the box plots for the 20-storey steel buildings and it is observed that the variation in peak response under the earthquake-induced loads is higher than that for the wind loads. The variation is triggered by a large dissimilarity in the spectral parameters of the input ground-motions, although the PGA of ground-motions are not differed substantially. Here, the mean values of the responses are compared and percentage difference in the responses are provided to understand the effectiveness of the passive control devices. Under the earthquake excitations, considering the mean value, the acceleration and base shear responses increase from 20% to ~40% for the SBF as compared to the MRF; whereas, the drift and displacement responses decrease from 2% to ~8%. The responses also decrease from ~24% to 47% for the FVDF and ~22% to 54% for the VEDF under the earthquakes. Moreover, percentage difference in the mean and median values of the responses are compared herein to demonstrate spread and skewness in the responses. The percentage difference of mean and median for the plots show that the difference in spread is mostly in the range of 10–54% for the responses of the steel MRF to VEDF, with the least skewness (8.10%) in top floor acceleration ($\ddot{x}_*$) of the FVDF and the highest skewness (53.30%) in drift (δ) of the VEDF. On contrary, under the wind excitations, almost all the responses decrease significantly, and the decrease is observed to be from ~9% to ~70%. However, the drift in the VEDF increases by 14% as compared to that in the steel MRF building. Moreover, the percentage difference in mean and median shows that the difference in spread lies from 1% to 10% for the responses obtained for the steel MRF to VEDF, with the least (1.2%) and the highest (~10%) skewness respectively observed in top floor displacement (x_*) and acceleration ($\ddot{x}_*$) of the VEDF. The VEDF provides the least response for the most cases, as the addition of stiffness and damping collectively influenced the response reduction under the action of the wind loads.

Fig. 6 shows the distribution of peak responses for the 25-storey steel building, and it is observed that the mean of the peak responses for the steel SBF increases significantly from 17% to ~90%; however, the peak drift response decreases substantially by ~17% under the earthquake ground excitations. The base shear in the controlled frames also increases relatively due the added stiffness forces. The responses for the FVDF and VEDF have reduced relatively and the differences in the responses for the controlled FVDF and VEDF are observed to be ~5% to 32% and ~5% to 36%, respectively. The difference in mean and median is the least (5%) for the top floor acceleration in the VEDF; whereas, the highest difference (~48%) is observed for the drift response in the FVDF. The response reduction as well as skewness for 20-storey building are compared with the 25-storey, which shows that the reduction and spread of responses in 25-storey building are relatively less under the earthquake-induced loadings. Under the wind excitations, the percentage difference in the responses observed from the mean is ~12% to 91%, except for the base shear response in the VEDF. The base shear in the VEDF increases significantly, which clearly indicates a contradictive behavior as compared to the responses obtained under the earthquakes. The possible reason for such contradiction is the participation of the higher modes of the 20- and 25-storey frames installed with the VED and owing to relatively reduced flexibility. The additional damping plays significant role in the response reduction of the inter-storey drift and displacement under the seismic action; however, the additional stiffness tends to increase the acceleration and base shear responses in the structures. On the other hand, the addition of damping is almost ineffective in the inter-storey drift response reduction under the action of the wind loads and nearly so for displacement response control. Hence, it is remarkable to note the ineffectiveness of the passive control systems in the VEDF that amounts to rather increased wind response. Therefore, it is concluded that the additional damping characteristics of the controlled steel buildings assist in response reduction under the earthquake-induced loads; on the contrary, the additional stiffness reduces the response under the action of the wind loads. This conclusion is crucial in assessing vibration control techniques for dynamic response mitigation of civil structures under multiple hazards.

Another important observation noticed herein is, as the dataset of earthquake and wind comprise of excitations ranging from lower to higher intensity, the additionally damped FVD device may not reduce the response significantly under the small earthquake and wind loads. Since velocity is proportional to the stroke of the damper, under a small earthquake or wind load, the displacement and velocity are small. As a result, the damping force is consequently small and the resulting effect in such cases can be found limited. Moreover, the additional stiffness induced in SBF helps in significant reduction in the response for the 25-storey building, as the structure is relatively flexible to meet the performance criteria under the wind loadings. Thus, in such circumstances, the effectiveness of a control strategy differs in the case-specific conditions. However, there exist situations where the selection of the control devices against a particular hazard has proven to be detrimental for the other hazard. Therefore, such tradeoff in the structural behaviors calls for a careful selection of the passive control devices for a structure considering possible multi-hazard scenarios.

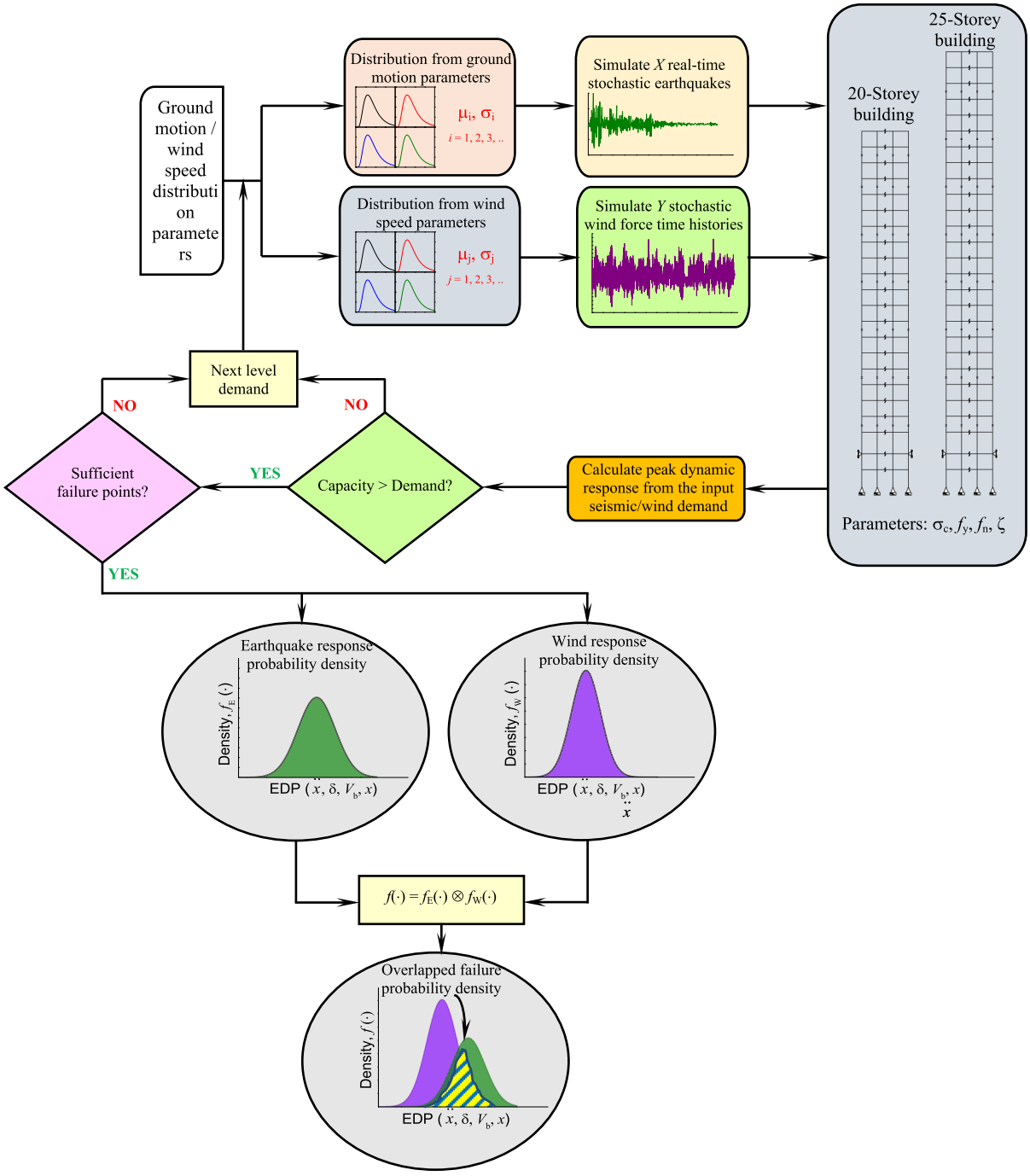

Fig. 4. Flowchart for the multi-hazard assessment of the steel buildings proposed through this study.

6.2. Failure density plots for steel buildings

Effectiveness of the passive control devices is also assessed from the overlapped failure probability density functions (PDFs) of the 20- and 25-storey steel buildings under the multi-hazard scenario, as shown from Figs. 7 through 10. The response quantities follow lognormal distribution, and in this regard, some of the mean quantities may assume negative values owing to logarithmic treatment of the actual mean values. The overlapped area indicates the failure under both the hazards, and also indicates the degree of effectiveness of the passive devices installed in the steel buildings. Fig. 7 shows the failure PDFs of the peak response for the top floor acceleration and inter-storey drift of the 20-storey steel buildings under the action of the two dynamic loading conditions. From the PDFs of the top floor acceleration, the highest mean is observed for the SBF under the earthquake-induced loads. The obtained mean values are lower for the SBF as compared to the MRF under the action of the wind loads. The overlapped area of the PDFs for the SBF (0.01) is lesser than that of the MRF (0.1) under these dynamic loads. Therefore, the probability of failure is lower for the SBF as compared to that for the MRF under the multi-hazard scenario. The wind loads have insignificant influence on the top floor acceleration response of the FVDF and VEDF for the considered performance level.

From the failure PDFs of the inter-storey drift, the least mean is observed for the VEDF under the earthquake excitations. The significant response reduction in the inter-storey drift is achieved due to the influence of combined action of stiffness and damping. A substantial reduction in the mean inter-storey drift is observed for the SBF under the action of the wind loads. However, there is a significant increase in the

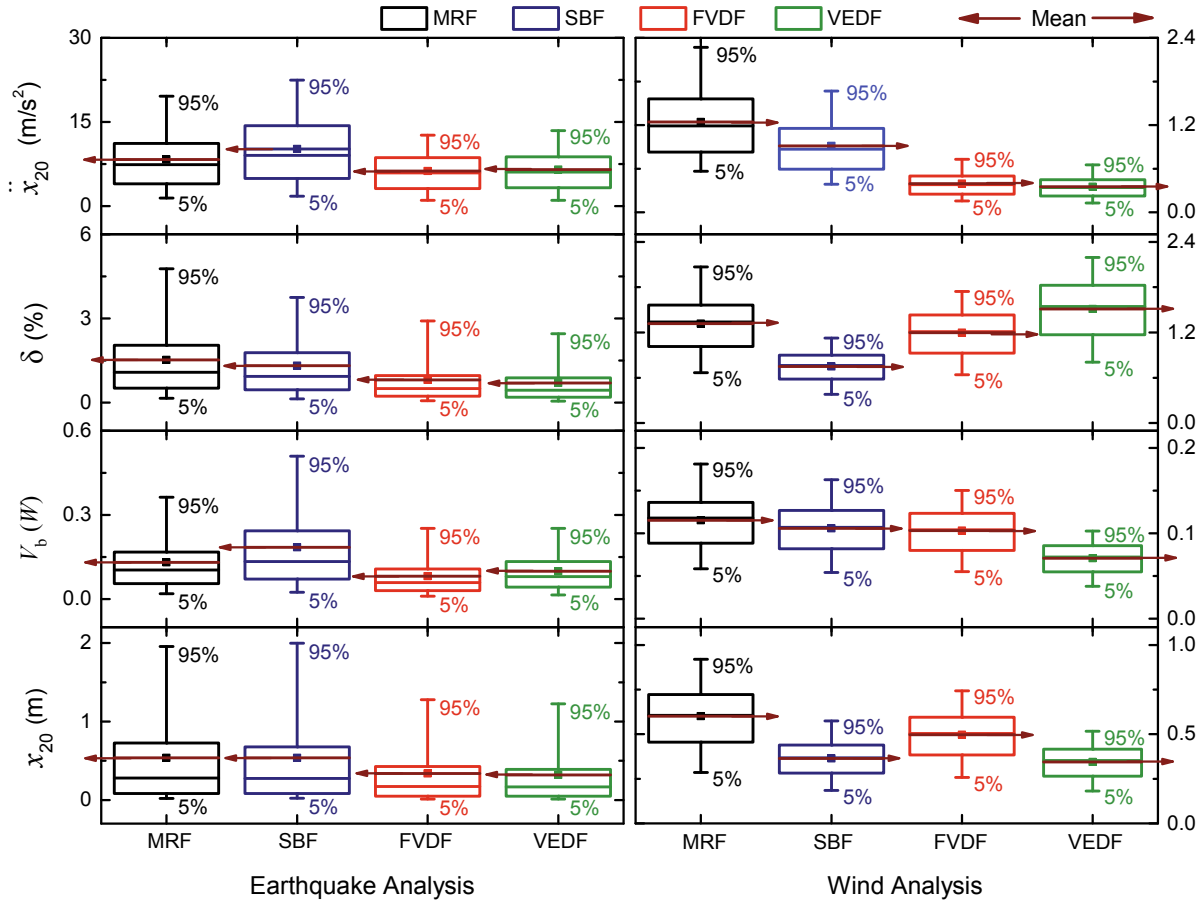

Fig. 5. Box plots representing the distribution of the response data for the 20-storey steel buildings under the earthquake and wind imparted loads.

mean inter-storey drift for the VEDF, which indicates amplified response as compared to the MRF under the action of the wind loads. The amplification of the response is due to the participation of the higher modes of the relatively stiffer frame, which in turn increases the response in the VEDF. The overlapped probability of failure for the VEDF (0.66) is observed to be significantly large as compared to the other buildings, with the SBF having the least value (0.15). Therefore, it is evident that the response control systems capable to limit the large responses for a particular hazard, may conversely attract increased force against the other hazard.

From Fig. 8, it is observed that mean of the PDFs for base shear in the SBF increased substantially under the earthquake-induced load. On the contrary, the base shear response decreased substantially under the wind load. The lowest mean of base shear response is observed for the VEDF owing to the contributions from the additional stiffness under the earthquake and wind loadings. The overlapped probability of failure for the FVDF (0.47) is almost the same as that of the MRF (0.46) for the base shear response. Therefore, if the buildings are equipped with the passive response control devices designed for the earthquake hazard by incorporating additional damping, exhibiting substantial seismic response reduction; it is not necessary that, in case of the wind hazard, similar dynamic response reduction can be achieved.

The PDFs of top floor displacement show that the FVDF has the least mean under earthquakes. The top floor displacement response is the highest for the SBF. Since high stiffness favors the dynamics of the framed structures under wind loads, no peak response reaches or exceeds the performance limits for the SBF as well as for the VEDF. The overlapped failure for the FVDF (0.16) is less than that for the MRF (0.20). The ineffectiveness of the FVD for the multi-hazard scenario in case of earthquake and wind is clearly observed, and hence, careful selection of the passive response control devices is utmost necessary from viewpoints of the multiple hazard exposure.

The standard deviations observed in Figs. 7 and 8 indicate that the wind responses have a lesser spread as compared to the seismic responses. The increased standard deviations of the seismic responses give an indicative measure of the variation in the spectral nature of the ground-motion excitations, although the ground-motions are observed to have closely matched PGAs. Therefore, it can be concluded that the additionally damped passive control system (FVD) is rather effective, although insignificant in mitigating the responses considered, as observed from the minor differences in the overlapped values of the failure PDFs. On the other hand, the added stiffness is effective in limiting the responses under both the dynamic loads considered herein. Therefore, the numbers indicate that the selection of a response control strategy is crucial for multi-hazard analysis and design of structures. In other words, the design of the response control systems should be able to cater for requirements from both the hazards in scenario-specific circumstances.

Figs. 9 and 10 illustrate the failure PDFs of the peak responses for the 25-storey steel buildings under the multiple dynamic loads. The counteracting effects of the passive devices are observed with increase in height of the steel buildings installed with the passive control devices. The top floor acceleration for the SBF has the highest mean under the earthquake-induced loads comparatively, as observed from Fig. 9, which is not the case (highest) under the action of the wind loads. The response substantially reduced for the SBF under the action of the wind loads. No peak response is observed to reach or exceed the performance limits for the FVDF and VEDF under the action of the wind loads. The overlapped failure probability for the SBF (0.05) is significantly low as compared to the MRF (0.11).

From the PDFs of the inter-storey drift, a higher mean is obtained for the SBF under the earthquake-induced loads; whereas, the mean is

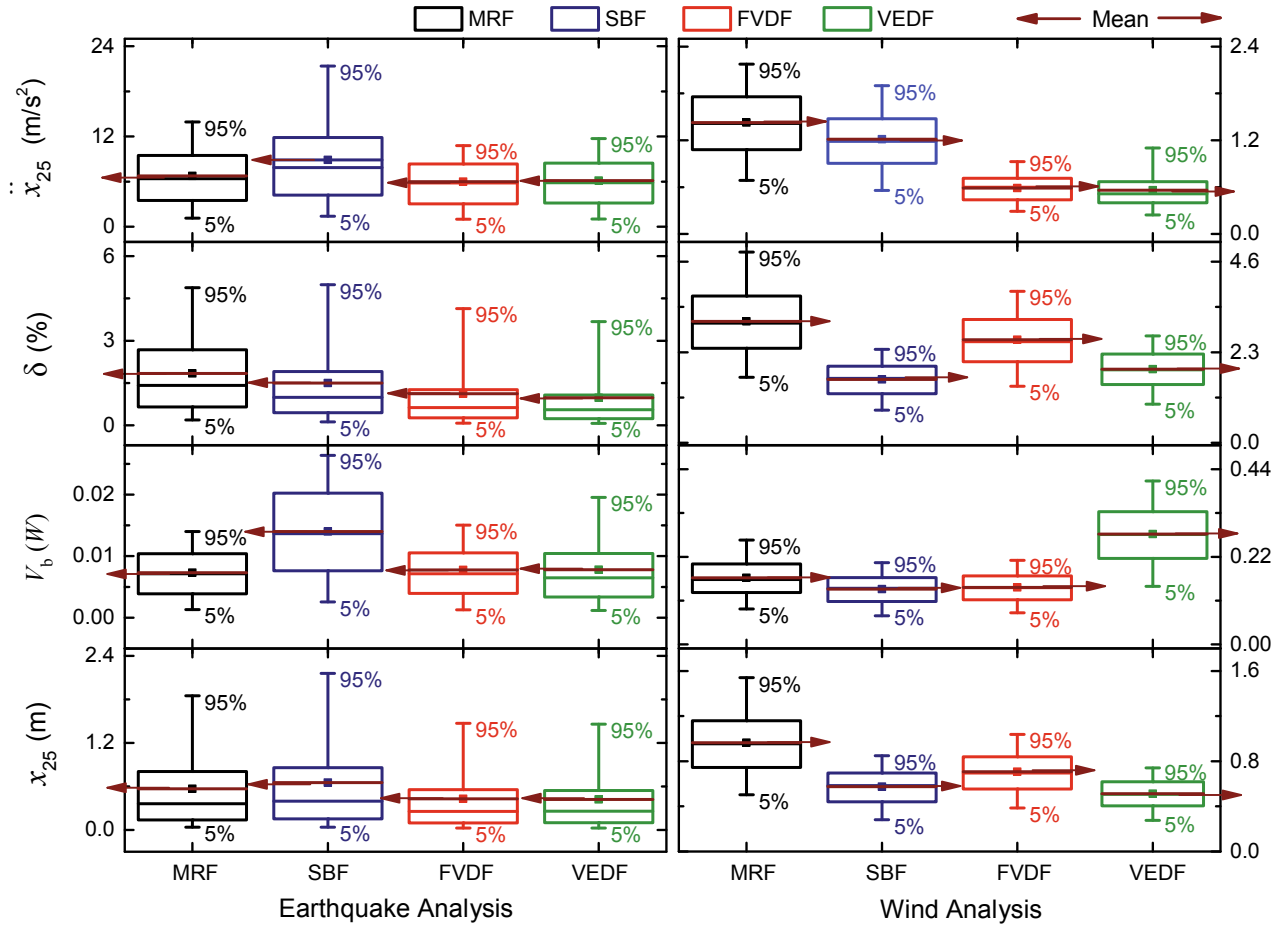

Fig. 6. Box plots representing the distribution of the response data for the 25-storey steel buildings under the earthquake and wind imparted loads.

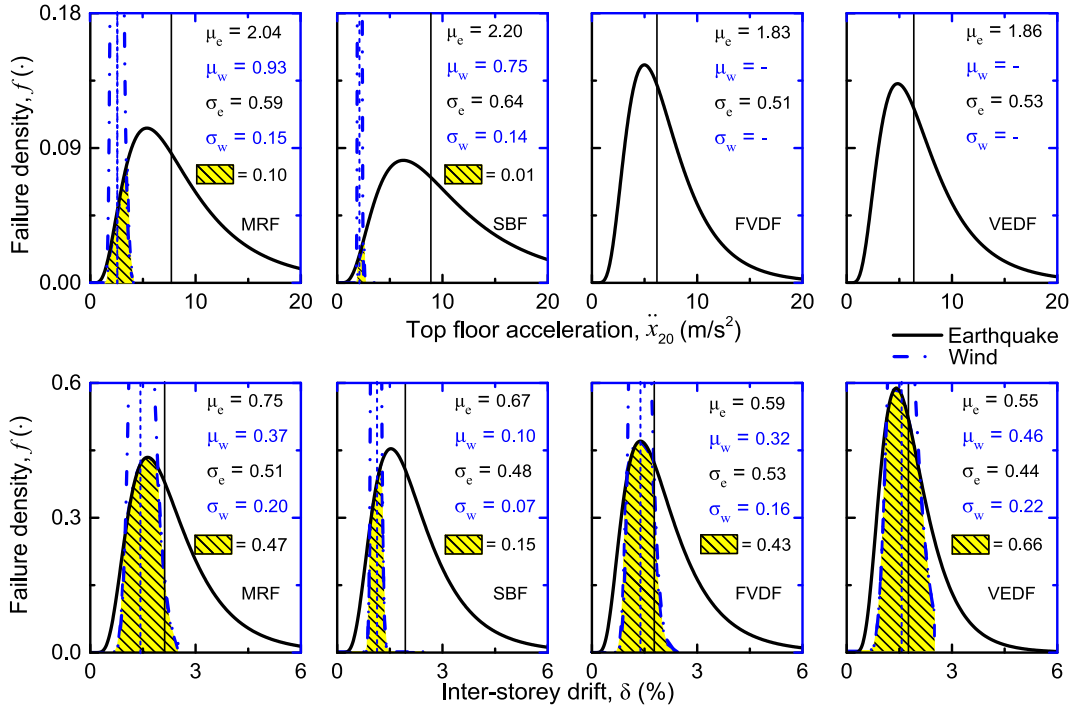

Fig. 7. PDFs of failure for limit states of the top floor acceleration and inter-storey drift for the 20-storey steel buildings under the earthquakes and winds.

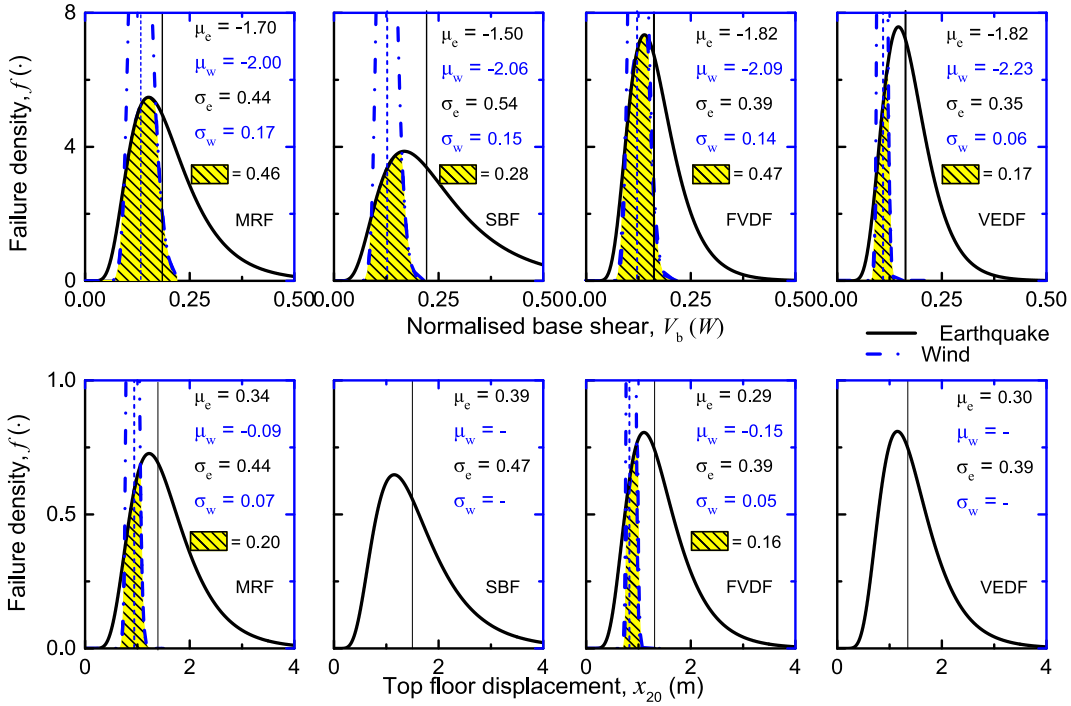

Fig. 8. PDFs of failure for limit states of the normalized base shear and top floor displacement for the 20-storey steel buildings under the earthquakes and winds.

the lowest under the action of the wind loads. As observed earlier, the supplemental damping helps in significant response reduction under the earthquake-induced load and the added stiffness helps in significant response reduction under the action of the wind loads. Considering drift in the steel buildings, the overlapped failure probability computed for the building indicates that the overlapped probability of failure is the least for the SBF (0.56) when assessed under the earthquake and wind imparted loads, and marginally higher for the FVDF and VEDF (both 0.64). These numbers clearly show that using a specific passive control device may not explicitly yield response reduction under the other hazard significantly, instead at times it may increase, which otherwise depends on the structural and loading dynamics of the system.

From the PDFs shown in Fig. 10, it is observed that no peak response has reached or exceeded the chosen performance limits for the seismic base shear under the earthquake hazard. Under the action of the wind loads, the least mean is observed in case of the SBF, while the highest mean is observed in case of the VEDF. It is evident that the peak base shear response in the VEDF increases significantly under the wind

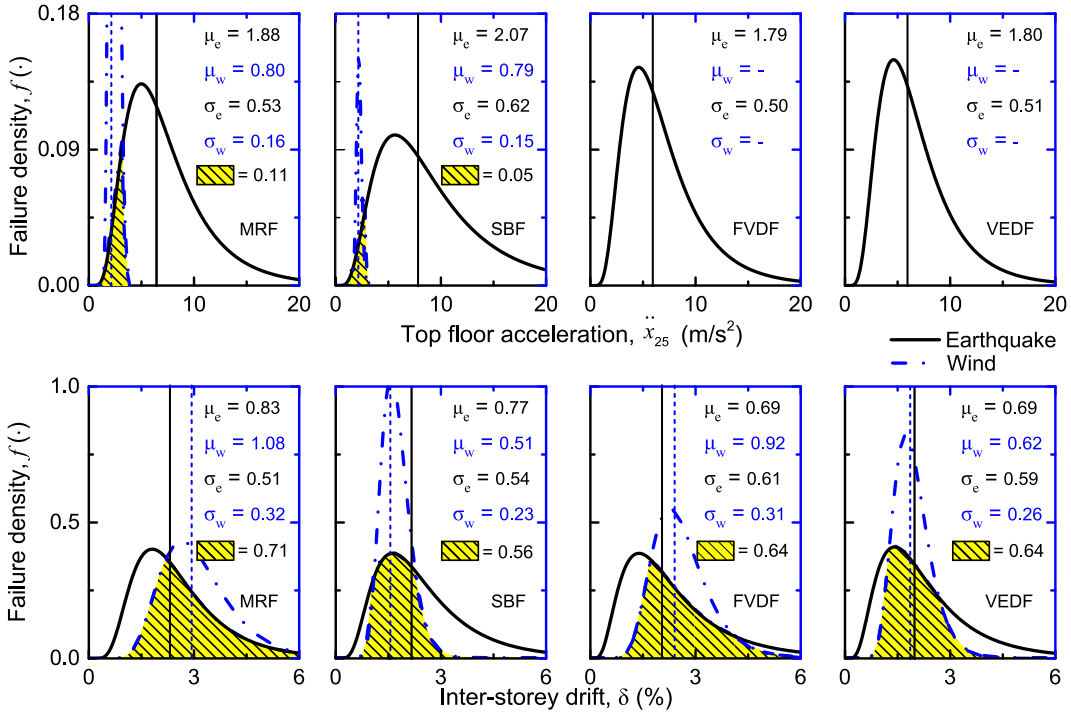

Fig. 9. PDFs of failure for limit states of the top floor acceleration and the inter-storey drift limit states for the 25-storey steel buildings under the earthquakes and winds.

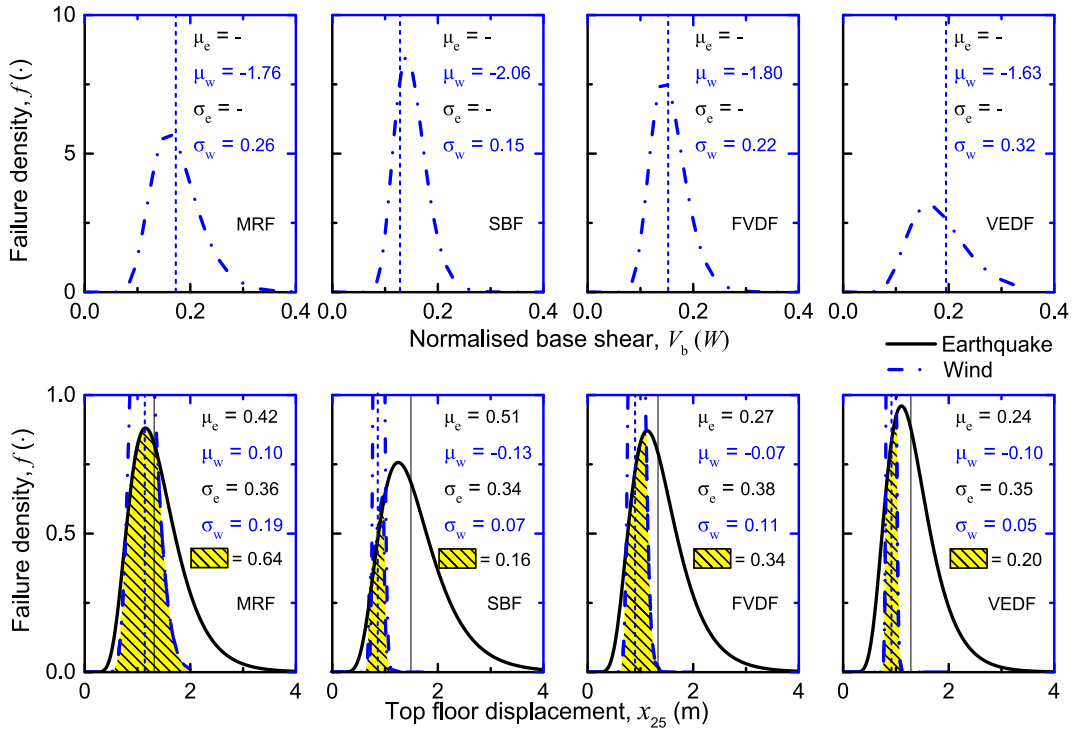

Fig. 10. PDFs of failure for limit states of the normalized base shear and top floor displacement limit states for the 25-storey steel buildings under the earthquakes and winds.

hazard, indicating relative ineffectiveness of the response control system employed.

The PDFs obtained for the top floor displacement show a similar trend as that of the inter-storey drift. From the mean of the response, it is inferred that, additional damping and stiffness is effective in minimizing the response mostly under the earthquake and wind loads, respectively. The probability of failure in case of the VEDF, with added stiffness and damping through the control device, is comparatively lower (0.20) as compared to that for the MRF (0.64).

The standard deviations obtained for the PDFs as observed in Figs. 9 and 10 highlight that the spread of the responses under the wind excitations is substantially low as compared to that for the seismic responses. Such difference shows that the variability in the spectral parameters of the considered loadings could affect the distribution of the responses. Therefore, in order to judge the effectiveness of the passive control strategies, a performance limit of ± 5% is set, which on exceeding the limit on either side would indicate the effectiveness or ineffectiveness of the control devices, i.e., robustness of the system. Table 5 highlights the effectiveness of the strategies quantified from the overlapped probability distribution plots for the 20- and 25-storey steel structures. It is observed that the VED is ineffective (< 5%) in controlling the inter-storey drift response in the 20-storey building under the multiple hazard scenario. Moreover, the use of FVD to control the base shear response in the 20-storey building is undesirable, although not ineffective, to control the response under the multiple hazards. It is concluded that the passive control systems are quite efficient in the context of a particular hazard considered; however, the converse effect may be observed for the other hazard. Therefore, apart from the investigation of cost effectiveness, such assessment strategy becomes one of the key approaches for selection of the passive devices and design for a structure, duly considering the multi-hazard effects.

Table 5
Effectiveness of the passive control devices under the multi-hazard scenario of earthquake and wind.

Building Frame	Response	SBF	FVDF	VEDF
20-storey	$\ddot{x}_{20}$	+90%	–	–
	δ	+68%	+8%	−40%
	V_b	+39%	−2%	+63%
	x_{20}	–	+20%	–
25-storey	$\ddot{x}_{25}$	+55%	–	–
	δ	+21%	+10%	+10%
	V_b	–	–	–
	x_{25}	+75%	+47%	+69%

+ indicates effectiveness; − indicates ineffectiveness.

6.3. Fragility curves of steel buildings

The conditional probability of failure (p_f) is represented by the fragility curves that denote peak response reaching or exceeding the chosen limit states under the earthquake and wind hazards. Fig. 11 shows the conditional probability of failure (p_f) in terms of the fragility curves for the 20-storey steel building without and with the passive control devices under the earthquake and wind imparted loads. The conditional failure probability of the SBF for the top floor acceleration is observed to be the highest under all intensity levels (PGA) of the earthquake-induced loads. The least failure probability is observed for the FVDF, which indicates the effectiveness of the added damping in response reduction. On the other hand, the conditional failure probability is lower for the SBF comparatively under the action of the wind loads. Hence, for the top floor acceleration, the SBF has the highest probability of failure under earthquake loads; however, failure probability substantially decreased under the wind loads.

For the limit state inter-storey drift, a reduction in the conditional failure probability is observed for the controlled buildings under the earthquake hazard, and is almost the same at all intensity levels. On the other hand, substantial decrease in the conditional probability of failure is observed for the SBF as compared to the FVDF and VEDF under the wind hazard. Interestingly, the conditional failure probability of the VEDF is increased significantly under the action of the wind loads. The addition of the supplemental energy dissipating devices has actually

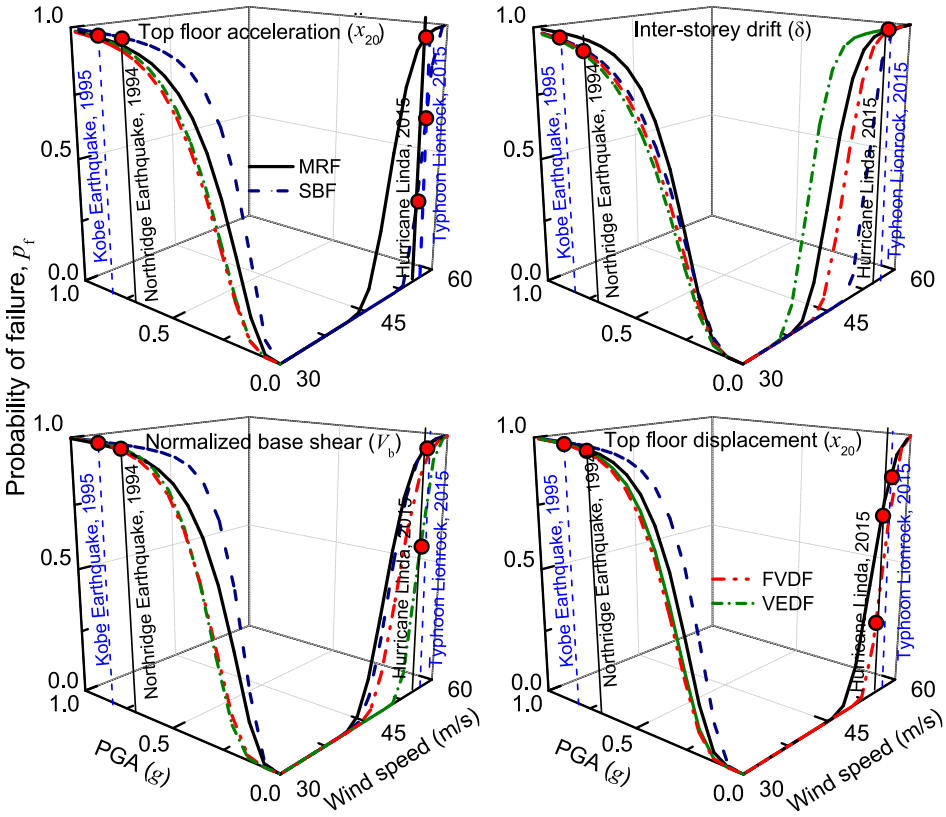

Fig. 11. Fragility curves of the 20-storey steel buildings for given limit states under the earthquakes and winds.

worsened the response against a particular hazard, which mandates careful selection of the passive control device and its characteristic parameters for the dynamic response control.

For the base shear, the SBF has the highest conditional probability of failure under the earthquake-induced loads; however, relatively lower failure probability for the SBF is observed under the action of the wind loads. It is further observed that there is a steep increase in the slope of the fragility curve indicating a large increase in the failure probability with a small increase in the PGA, i.e., earthquake intensity.

The conditional probability of failure for the top floor displacement has increased significantly for the SBF under the earthquake-induced loads. The contribution of the response from the higher modal frequencies in the relatively stiffer structure becomes responsible for the increased response. The least probability of failure is observed in the FVDF, as the effect of damping is significant in response reduction under the seismic action without making the structure stiffer. As the addition of stiffness is effective in response reduction under wind loads, no response values reaching or exceeding the chosen performance limits are obtained for the SBF and VEDF.

The conditional probability of failure for the steel buildings in case of the events where probability of a ground-motion and wind speed exceeding 0.3 *g* and 33 m/s in 100 years is studied. The conditional failure probabilities for acceleration limit state under the earthquake-induced loadings are obtained as 0.69, 0.90, 0.51, and 0.52 respectively for the MRF, SBF, FVDF, and VEDF buildings. Similarly, for the inter-storey drift, the respective conditional failure probabilities are obtained as 0.7, 0.54, 0.47, and 0.46. For the limit state of base shear, the respective failure probabilities are obtained as 0.75, 0.96, 0.50, and 0.50, and the probabilities of failure for the limit state of displacement are 0.70, 0.88, 0.56, and 0.55, respectively for the MRF, SBF, FVDF, and VEDF buildings under the ground-motion excitations. Under the design wind speed, no limit state exceeds the threshold value except for the inter-storey drift in the VEDF, which is obtained as 0.40. The overall reduction in the failure probability obtained from installing the FVD and VED in the structure range from 20% to 35%; whereas, the conditional probability of failure increases from 22% to 33% when installed with the steel bracings under the earthquake-induced loadings. Hence, a particular strategy effective to control large response against a specific hazard is showing insignificant effect against the another hazard, which underlines the need to adopt holistic approach for multi-hazard protection of structures.

From the conditional probability of failure plots for the 25-storey steel buildings shown in Fig. 12, it is observed that the FVD and VED are effective in minimizing the seismic response efficiently at the lower PGA levels for the limit state of top floor acceleration. However, it is seen that the conditional failure probability curves for the controlled buildings have steeper slopes than that for the MRF. This indicates the ineffectiveness of the passive control scheme, as marginal increase in the PGA increases the failure probability quite drastically. The effectiveness of the steel bracing is observed under lower and moderate wind speeds; however, the steeper slope indicates ineffectiveness of the passive control system.

The conditional failure probability curves of the inter-storey drift show that significant reduction in the probability of failure is observed for the passively controlled buildings, with the FVDF showing the least failure probability. Failure probability for the inter-storey drift is observed to be the least for the SBF as higher stiffness favors significant wind response reduction. Failure probability is not observed for the base shear under the earthquake-induced loads as no peak response reached or exceeded the chosen limit state. The probability of failure is observed to be the least for the SBF under the action of the wind loads. However, the failure probability for the VEDF is observed to be the highest, thereby the control strategy chosen fails to deliver the objective, which essentially is intended to lessen the peak response.

For the top floor displacement, the SBF has the highest conditional failure probability under the earthquake-induced loads; however, the least failure probability is observed under the action of the wind loads. The FVDF shows lesser probability of failure as compared to the MRF

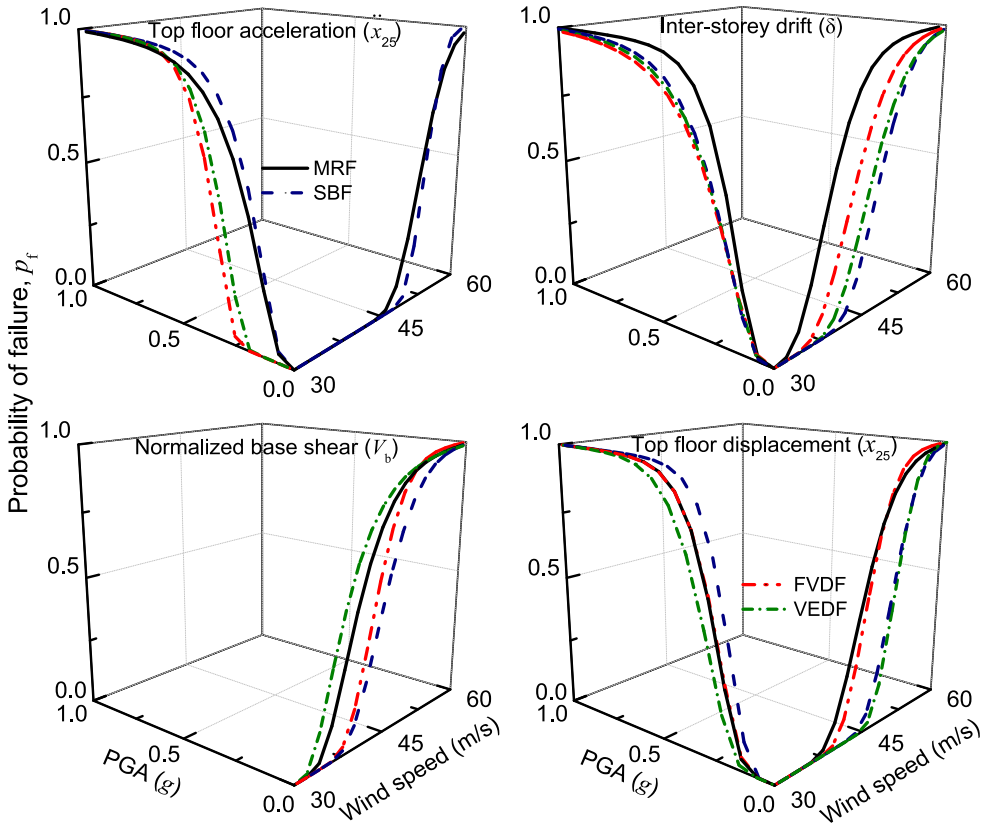

Fig. 12. Fragility curves of the 25-storey steel buildings for given limit states under the earthquakes and winds.

under the earthquake-induced loads; on the contrary, it shows negligible effect against the wind loads. The conditional failure probability for the top floor displacement shows a significant effect of the added damping to control the large deformations under the earthquakes. On the other hand, the effect of additional stiffness is substantial in minimizing the response under the wind hazard and is observed from the failure plot of the top floor displacement.

Similar to the 20-storey steel building, conditional probabilities of failure are also obtained for the 25-storey building for the design earthquake and wind hazards. For the limit state of acceleration, the conditional failure probabilities under the random earthquake loads are determined as 0.86, 0.92, 0.50, and 0.70 respectively for the MRF, SBF, FVDF, and VEDF structures. The conditional failure probabilities for the limit state of drift and top floor displacement are obtained as 0.97, 0.78, 0.77, and 0.77; and 0.82, 0.98, 0.81, and 0.7 respectively for the structures. Under the wind excitations, for the design wind speed of 33 m/s, no probability of failure for limit states of acceleration and displacement is obtained. On the other hand, the conditional failure probabilities for the limit state of drift and base shear are respectively obtained as 0.25, 0, 0.06, and 0; and 0.27, 0.05, 0.06, 0.53 for the MRF, SBF, FVDF, and VEDF frames. Under the earthquakes, the overall reduction in the failure probability for the FVD and VED ranges from 12% to 42%; whereas, the failure probability increases from 7% to 20% when installed with the steel bracings, i.e., addition of stiffness only. On contrary, the SB and FVD devices reduce the conditional failure probabilities under wind responses from 76% to 100%; whereas, the failure probability using the FVD increases by 96%. Therefore, it is evident that, although, a response control strategy is effective against a particular hazard, the vulnerability against the other hazard may increase substantially with the same control scheme, mandating holistic multi-hazard scenario-based design of the dynamic response control devices.

7. Conclusions

Herein, a novel probabilistic approach is developed and presented to assess the effectiveness of passive control devices, viz., steel bracings, fluid viscous dampers, and viscoelastic dampers installed in the 20-storey and 25-storey steel buildings under multi-hazard scenario of earthquake and wind. Variation in the dynamic response are studied using box plots. Moreover, probability of failure is assessed through the development of overlapped probability density functions and fragility curves to evaluate the effectiveness of the control systems. The proposed methodology is best suited for structures that have the dominant modal frequencies within the overlapped critical frequency range of earthquakes and winds. In such cases, there exist several structures designed to resist seismic forces in its design life, which may become vulnerable against wind loadings, and vice-versa. These structures are required to be assessed and designed carefully to mitigate the responses against the multi-hazard effects of earthquakes and winds during the service life. The major conclusions drawn from this investigation are summarized below.

1. The probability of failure for a structure experiencing high-amplitude seismic hazard and a maximum wind speed lying within the critical frequency band during the design life varies largely for different damper schemes. Hence, based on the site-specific conditions and probability of occurrence of each hazard, selection of proper passive control scheme and its design is essential to alleviate large responses in structures prone to multi-hazard scenario.
2. The vulnerability curves demonstrate that the passive devices are effective to control the response at the lower level of demand; however, the same passive devices may not necessarily be suitable for the higher demand levels. The failure probability obtained from the fragility curves for the controlled buildings have relatively

steeper slopes. With marginal increase in the intensity level, the failure probability increases quite drastically, thus indicating the ineffectiveness of the control system at higher intensity levels.

3. The design of the passive control devices employing additional damping may account for the performance of the structures under the multi-hazard scenario. As velocity is proportional to stroke of the damper under a small earthquake or wind load, the induced displacement and velocity are small. As a result, the damping force is small and consequently their effect in such cases can be found limited.
4. The variability in either of the demands affects the failure probability of the passively controlled structures extensively, especially under the seismic ground-motions. The uncertainty is mostly triggered by a significant variation in the spectral parameters/ frequency content of the input ground-motions, although the intensity level, i.e., PGA of ground-motions are not differed substantially. As the present study is based on a specific region, more refinement of this framework is required to develop the multi-hazard assessment of structures in a holistic manner.

References

[1] Bisadi V, Padgett JE. Explicit time-dependent multi-hazard cost analysis based on parameterized demand models for the optimum design of bridge structures. Comput Aided Civ Infrast Eng 2015;30(7):541–54.
[2] Cha, E.J., and Ellingwood, B.R. (2013), “Acceptance of risk due to competing wind and earthquake hazards”, 11th International Conference on Structural Safety and Reliability (ICOSSAR), New York (NY), USA.
[3] Chandrasekaran S, Banerjee S. Retrofit optimization for resilience enhancement of bridges under multi-hazard scenario. J Struct Eng ASCE 2015:C4015012.
[4] Chao S-H, Karki NB, Sahoo DR. Seismic behavior of steel buildings with hybrid braced frames. J Struct Eng (ASCE) 2013;139(6):1019–32.
[5] Chulahwat A, Mahmoud H. A combinatorial optimization approach for multi-hazard design of building systems with suspended floor slabs under wind and seismic hazards. Eng Struct 2017;137:268–84.
[6] Crosti C, Duthinh D, Simiu E. Risk consistency and synergy in multi-hazard design. J Struct Eng (ASCE) 2011;137(8):844–9.
[7] Dogruel, S., and Dargush, G. (2008), “A framework for multi-hazard design and retrofit of passively damped structures”, AEI Conference, Building Integration Solutions, Denver, Colorado (CO), USA.
[8] Duthinh D, Simiu E. Safety of structures in strong winds and earthquakes: multi-hazard considerations. J Struct Eng (ASCE) 2010;136(3):330–3.
[9] Ellingwood BR, Tekie PB. Wind load statistics for probability-based structural design. J Struct Eng (ASCE) 1999;125(4):453–63.
[10] Ellingwood BR, Rosowsky DV, Li Y, Kim JH. Fragility assessment of light-frame wood construction subjected to wind and earthquake hazards. J Struct Eng (ASCE) 2004;130(12):1921–30.
[11] Fitzgerald B, Basu B. A monitoring system for wind turbines subjected to combined seismic and turbulent aerodynamic loads. Struct Monitor Maint 2017;4(2):175–94.
[12] Fur L-S, Yang HTY, Ankireddi S. Vibration control of tall buildings under seismic and wind loads. J Struct Eng (ASCE) 1996;122(8):948–57.
[13] Gehl P, D’Ayala D. Development of Bayesian networks for the multi-hazard fragility assessment of bridge systems. Struct Saf 2016;60:37–46.
[14] Guzman-Morales J, Gershunov A, Theiss J, Li H, Cayan D. Santa ana winds of southern california: their climatology, extremes, and behavior spanning six and a half decades. Geophys Res Lett 2016;43(6):2827–34.
[15] Jiuhong J, Jianye D, Yu W, Hongxing H. Design method for fluid viscous dampers. Arch Appl Mech 2008;78(9):737–46.
[16] Kaimal JC, Wyngaard JC, Izumi Y, Cote OR. Spectral characteristics of surface-layer turbulence. J R Meteorol Soc 1972;98:563–89.
[17] Kameshwar S, Padgett JE. Multi-hazard risk assessment of highway bridges subjected to earthquake and hurricane hazards. Eng Struct 2014;78:154–66.
[18] Kappes MS, Keiler M, Elverfeldt KV, Glade T. Challenges of analyzing multi-hazard risk: a review. Nat Hazards 2012;64(2):1925–58.
[19] Kaur N, Matsagar VA, Nagpal AK. Earthquake response of mid-rise to high-rise buildings with friction dampers. Int J High-Rise Build 2012;1(4):311–32.
[20] Kodakkal A, Saha SK, Sepahvand K, Matsagar VA, Duddeck F, Marburg S. Uncertainties in dynamic response of buildings with non-linear base-isolators. Eng Struct 2019;197:109423https://doi.org/10.1016/j.engstruct.2019.109423.
[21] Komendantova N, Mrzyglocki R, Mignan A, Khaza B, Wenzel F, Patt A, et al. Multi-hazard and multi-risk decision-support tools as a part of participatory risk governance: feedback from civil protection stakeholders. Int J Disaster Risk Reduct 2014;8:50–67.
[22] Korswagen PA, Jonkman SN, Terwel KC. Probabilistic assessment of structural damage from coupled multi-hazards. Struct Saf 2019;76:135–48.
[23] Lago A, Wood A, Trabucco D. Damping technologies for tall buildings: new trends in comfort and safety. Butterworth-Heinemann, Elsevier, UK: Damping Technologies for Tall Buildings; 2018.
[24] Lee D, Taylor DP. Viscous damper development and future trends. Struct Des Tall Build 2001;10(5):311–20.
[25] Lewandowski R, Pawlak Z. Dynamic analysis of frames with viscoelastic dampers modelled by rheological models with fractional derivatives. J Sound Vib 2010;330(5):923–36.
[26] Li Y, Ahuja A, Padgett JE. Review of methods to assess, design for, and mitigate multiple hazards. J Perform Constr Facil (ASCE) 2012;26(1):104–17.
[27] Li Y, Ellingwood BR. Framework for multi-hazard risk assessment and mitigation for wood-frame residential construction. J Struct Eng (ASCE) 2009;135(2):159–68.
[28] Mardfekri M, Gardoni P. Multi-hazard reliability assessment of offshore wind turbines. Wind Energy 2015;18(8):1433–50.
[29] Martinez-Rodrigo M, Romero ML. An optimum retrofit strategy for moment resisting frames with nonlinear viscous dampers for seismic applications. Eng Struct 2003;25(7):913–25.
[30] Matsagar VA, Jangid RS. Viscoelastic damper connected to adjacent structures involving seismic isolation. J Civil Eng Manage 2005;11(4):309–22. https://doi.org/10.1080/13923730.2005.9636362.
[31] Moria Y, Katoa T, Muraib K. Probabilistic models of combinations of stochastic loads for limit state design. Struct Saf 2003;25(1):69–97.
[32] Nikellis A, Sett K, Whittaker AS. Multihazard design and cost-benefit analysis of buildings with special moment-resisting steel frames. J Struct Eng (ASCE) 2019;145(5):04019031.
[33] O'Connor JM, Ellingwood BR. Site-dependent models of earthquake ground motion. Earthq Eng Struct Dyn 1992;21(7):573–89.
[34] Ohtori Y, Christenson RE, Spencer BF, Dyke SJ. Benchmark problems in seismically excited nonlinear buildings. J Eng Mech (ASCE) 2004;130(4):366–85.
[35] Parsons T, Geist EL, Console R, Carluccio R. Characteristic earthquake magnitude frequency distributions on faults calculated from consensus data in California. J Geophys Res Solid Earth 2018;123(12):10761–84.
[36] Patil VB, Jangid RS. Response of wind-excited benchmark building installed with dampers. Struct Des Tall Special Build 2011;20(4):497–514.
[37] Pearce HT, Wen YK. Stochastic combination of load effects. J Struct Eng (ASCE) 1984;110(7):1613–29.
[38] Potra FA, Simiu E. Optimization and multihazard structural design. J Eng Mech (ASCE) 2009;135(12):1472–5.
[39] Reed DA, Friedland CJ, Wang S, Massarra CC. Multi-hazard system-level logit fragility functions. Eng Struct 2016;122:14–23.
[40] Roy T, Agarwal P. Comparison of damage index and fragility curve of RC structure using different Indian standard codes. J Struct Eng (SERC) 2016;43(1):1–9.
[41] Roy, T., Matsagar, V., 2017, “Multi-hazard assessment of steel buildings retrofitted with passive control devices”, 16th World Conference on Earthquake Engineering, Santiago, Chile.
[42] Roy T, Matsagar V. Effectiveness of passive response control devices in buildings under earthquake and wind during design life. Struct Infrastruct Eng 2019;15(2):252–68. https://doi.org/10.1080/15732479.2018.1547768.
[43] Saha SK, Matsagar VA, Jain AK. Seismic fragility of base-isolated water storage tanks under non-stationary earthquakes. Bull Earthq Eng 2016;14(4):1153–75. https://doi.org/10.1007/s10518-016-9874-y.
[44] Soong TT, Spencer BF. Active, semi-active and hybrid control of structures. Bull N Z Soc Earthq Eng 2000;33(3):387–402.
[45] Spencer, B.F., Christenson, R.E., and Dyke, S.J. (1999), “Next generation benchmark control problems for seismically excited buildings”, 2nd World Conference on Structural Control, New York (NY), USA.
[46] Tapia C, Padgett JE. Multi-objective optimization of bridge retrofit and post-event repair selection to enhance sustainability. Struct Infrastruct Eng 2016;12(1):93–107.
[47] Unobe ID, Sorensen AD. Multi-hazard analysis of a wind turbine concrete foundation under wind fatigue and seismic loadings. Struct Saf 2015;57:26–34.
[48] Venanzi I, Lavan O, Ierimonti L, Fabrizi S. Multi-hazard loss analysis of tall buildings under wind and seismic loads. Struct Infrastruct Eng 2018;14(10):1295–311.
[49] Venkittaraman A, Banerjee S. Enhancing resilience of highway bridges through seismic retrofit. Earthquake Eng Struct Dyn 2014;43(8):1173–91.
[50] Wen YK. Minimum lifecycle cost design under multiple hazards. Reliab Eng Syst Saf 2001;73(3):223–31.
[51] Wen YK, Kang YJ. Minimum building life-cycle cost design criteria. I: methodology. J Struct Eng (ASCE) 2001;127(3):330–7.
[52] Yilmaz T, Banerjee S, Johnson PA. Performance of two real-life California bridges under regional natural hazards. J Bridge Eng (ASCE) 2016;21(3):04015063.